XL CILAMCE
IBERO-LATIN AMERICAN CONGRESS ON COMPUTATIONAL METHODS IN ENGINEERING
NOVEMBER 11-14, 2019
Praiamar Natal Hotel & Convention Natal, RN-BRAZIL

NUMERICAL ANALYSIS AND APPLICATION ON COVARIANCE-DRIVEN STOCHASTIC SUBSPACE METHOD IN MODAL PARAMETERS IDENTIFICATION

Yeny V. Ardila
yva.2019@aluno.unila.edu.br
Ivan D. Gomez
ivan.araujo@unila.edu.br
Universidade Federal da Integração Latino-Americana
Av. Tancredo Neves, 6731 – Bloco 4, CEP 85867-970, Paraná / Foz do Iguaçu, Brasil
Jesús D. Villalba
jesus.villalba@javeriana.edu.co
Pontificia Universidad Javeriana
Carrera 7 No 40-62 – Bogotá D.C. - Colombia
Luis A. Aracayo
luis.aracayo@pti.org.br
Centro de Estudos Avançados em Segurança de Barragens

Abstract. The SSI-COV method (Covariance-driven Stochastic Subspace Identification) is a technique within time domain modal identification methods that uses ambient vibrations as the input forces for the identification of modal parameters (natural frequencies, damping ratios and vibration modes). In this method two alternatives are available for the identification of the state space transition matrix: a) applying the decomposition property of a shifted block Toeplitz correlation matrix or b) by applying the shift property of the observability matrix. In this research, the SSI-COV was applied for the determination of dynamic characteristics (natural frequencies and damping ratios) of a concrete block of the Itaipú Hydroelectric Dam. This dam is equipped with a monitoring system, currently in operation, which collects acceleration data. For the implementation, the method was programmed in the Python language and validated through two types of simulations in which the sensitivity of the method was evaluated. Then, for the identification of modal parameters of the concrete block, it was applied to the acceleration records from a sensor installed in it the two alternatives for identification. Finally, the obtained results from the two variants to compute the state transition matrix allowed us to define that applying the shift property of the observability matrix is more advantageous in terms of data accuracy and computational cost.

Keywords: Identification, concrete block, modal parameters.

1 Introduction

Due to the growth in the construction of large civil structures, it has become necessary to develop structural monitoring systems that allow real-time data to be obtained directly from the structure and thus support decisions that lead to keeping the structures at a high level of performance and safety [1]. Furthermore, due to technological advances in the treatment of information and sensors, the control of structures that were usually carried out by visual inspection techniques evolved with the emergence of new non-destructive methodologies based on different approaches such as deformations, stresses, acoustic emissions, ambient vibrations, etc [2].

Civil structures are excited by ambient vibrations (traffic, wind, microseisms). Methods based on this type of vibration allow the identification of the modal parameters of the structure (natural frequencies, damping ratios, vibration modes), based on the response of the excitation produced by the ambient, i.e. the modal identification is carried out under normal operating conditions, which is more advantageous in comparison with other methods [3,4]. These modal identification methods are based on the hypothesis that significant changes in the modal parameters of the structure provide information about structural health, because the modal properties are associated with the physical properties of the structure (mass, stiffness, damping).

According to Cunha et al. [5], methods using ambient vibrations assume that the input excitation is a white noise with an average Gaussian distribution of zero. Currently, these modal identification methods are divided into two main groups: Frequency domain and time domain methods [6]. The frequency domain methods can be non-parametric methods, while the methods in the time domain are all parametric methods. The time domain methods adjust mathematical models to dynamically idealize the system and are more efficient at automating the calculation, which is advantageous when a considerable amount of data is available. In the group of methods in the frequency domain, Frequency Domain Decomposition (FDD) [7] and Poly-Least Squares Complex Frequency Domain (P-LSCF) [8] are the two methods commonly used in the application of civil structures. On the other hand, SSI-COV and SSI-DATA are two methods that perform good in the time domain [9].

The Stochastic Subspace Identification SSI-COV method [9], has been applied in the identification of modal parameters in dams [1,10], bridges [11,12,13], wind towers [14] and buildings [15]. This method is based on covariance matrices of the measured structural responses time series, which are organized in a Toeplitz matrix. The corresponding algorithm explores the properties of stochastic systems [16] and involves the performance of a singular value decomposition and the resolution of a least-squares equation using Moore-Penrose pseudo-inverse [9]. In short, the main purpose of the SSI-COV is to identify a transition matrix A, which contains all the modal information. There are available two ways to compute this matrix A. The first one applying the shift property of the observability matrix [17] and the second applying the decomposition property of a shifted block Toeplitz correlation matrix. [18].

In this work, the SSI-COV method is applied to identify the natural frequencies and damping ratios of a concrete block of the Itaipú Hydroelectric Dam. The transition matrix A will be computed in the two ways described above with the aim of establishing if any of them offers advantages in terms of precision and computational cost.

2 Covariance-driven stochastic subspace method

The stochastic state-space model for a structure that is being excited by unmeasurable stochastic input forces has the following form:

$$\{x_{k+1}\} = [A]\{x_k\} + \{w_k\}, \tag{1}$$

$$\{y_k\} = [C]\{x_k\} + \{v_k\}, \tag{2}$$

where $\{x_k\} \in \mathcal{R}^{2nx1}$ is the state vector and $\{y_k\} \in \mathcal{R}^{lx1}$ is the measurement vector, $\{w_k\}$ and $\{v_k\}$ are unknown, nonetheless it is assumed that they have a discrete white noise nature with expected value equal to zero and that they have covariance matrices equal to:

$$E\left[\begin{pmatrix} w_p \\ v_p \end{pmatrix} \begin{pmatrix} {w_p}^T & {v_q}^T \end{pmatrix}\right] = \begin{pmatrix} Q & S \\ S^T & R \end{pmatrix} \delta_{pq}, \tag{3}$$

where E is the expected value operator and δ_{pq} is the Kronecker delta. The sub-indices in Eq. (1) and Eq. (2), correspond to discrete time sample numbering, related to the time through $t = (k-1)f_s^{-1}$, where f_s is the sampling frequency. The purpose of the SSI-COV algorithm is to identify the transition matrix A which contains all the modal information. The starting point of the method is to establish the data Hankel data matrix Eq. (4) and then form the block Toeplitz matrix by a multiplication between future and transpose of past measurements Eq (5).

$$[H] = \frac{1}{\sqrt{N}}\begin{bmatrix} y_1 & y_2 & \cdots & y_N \\ y_2 & y_3 & \cdots & y_{N+1} \\ \cdots & \cdots & \cdots & \cdots \\ y_i & y_{i+1} & \cdots & y_{i+N-1} \\ \hline y_{i+1} & y_{i+2} & \cdots & y_{i+N} \\ y_{i+1} & y_{i+3} & \cdots & y_{i+N+1} \\ \cdots & \cdots & \cdots & \cdots \\ y_{2i} & y_{2i+1} & \cdots & y_{2i+N-1} \end{bmatrix} = \begin{bmatrix} Y_p \\ \hline Y_f \end{bmatrix}, \tag{4}$$

$$[T]_{1|i} = \begin{bmatrix} [R_i] & [R_{i-1}] & \cdots & [R_1] \\ [R_{i+1}] & [R_i] & \cdots & [R_2] \\ \cdots & \cdots & \cdots & \cdots \\ [R_{2i-1}] & [R_{2i-2}] & \cdots & [R_i] \end{bmatrix} = Y_f(Y_p)^T, \tag{5}$$

where Y_p denotes the past measurements and Y_f denotes for the future measurements. The discrete correlation matrix with time lag i is defined as R_i and has the following factorization properties:

$$[R_i] = E[\{y_k\}\{y_{k-i}\}^T] = CA^{i-1}G, \tag{6}$$

where G is the next-step state and output covariance matrix $G = E[x_{k+1}{y_k}^T]$. The discrete correlation matrix can be estimated by employing *FFT* and *IFFT* or implemented with the Python function *numpy.correlate*, without normalization.

The Toeplitz matrix can be factorized into the extended observability matrix $O_i \in \mathcal{R}^{lix2n}$ and the reversed extended stochastic controllability matrix $\Gamma_i \in \mathcal{R}^{2nxli}$, as show below:

$$[T]_{1|i} = O_i\Gamma_i = \begin{bmatrix} C \\ CA \\ \cdots \\ CA^{i-1} \end{bmatrix}[A^{i-1}G \quad \cdots \quad AG \quad G]. \tag{7}$$

As the rank of O_i and Γ_i is 2n, then of Eq. (7) it can be concluded that the rank of $[T]_{1|i}$ is also 2n. The rank of $[T]_{1|i}$ is not less than 2n due to the noises in the observed data. Generally, singular values caused by noise are much lower than those caused by true data. To reduce the effects of noise, it is used the truncated decomposition of singular values, which converts the singular values caused by noise into zeros. This is a common method used in signal processing. Then, $[T]_{1|i}$ can be written as a decomposition of singular values in the following way:

$$T_{1|i} = USV^T = [U_1 \quad U_2]\begin{bmatrix} S_1 & 0 \\ 0 & S_2 \end{bmatrix}\begin{bmatrix} V_1 \\ V_2 \end{bmatrix}^T = U_1S_1{V_1}^T, \tag{8}$$

where U and V are orthonormal matrices, and S is a diagonal matrix containing positive singular values in descending order. The comparison of Eq. (7) and (8) shows that the observability and the controllability matrices can be calculated from the outputs of the SVD using, for instance, the following partition of the singular values matrix:

$$O_i = U_1 {S_1}^{1/2}, \tag{9}$$

$$\Gamma_i = {S_1}^{1/2} {V_1}^T. \tag{10}$$

From O_i matrices A and C can be obtained easily. The system matrix A can be computed by exploiting the shift structure of the extended observability matrix [19]:

$$\begin{bmatrix} CA \\ CA^2 \\ \cdots \\ CA^i \end{bmatrix} = \begin{bmatrix} C \\ CA \\ \cdots \\ CA^{i-1} \end{bmatrix} A \Leftrightarrow A = \begin{bmatrix} C \\ CA \\ \cdots \\ CA^{i-1} \end{bmatrix}^+ \begin{bmatrix} CA \\ CA^2 \\ \cdots \\ CA^i \end{bmatrix} = O_i(1{:}\,l(i-1),:)^+ O_i(l+1{:}\,li,:), \tag{11}$$

where + represents the Moore-Penrose pseudo-inverse of a matrix, which is used to solve least squares problems (minimizes the sum of the squared errors of the individual equations of an overdetermined system of equations).

A second possible way to compute the state transition matrix A [18] follows from the decomposition property of a shifted block Toeplitz matrix:

$$T_{2\,|\,i+1} = O_i A \Gamma_i\,, \tag{12}$$

where the shifted matrix $T_{2\,|\,i+1}$ has a similar structure as $T_{1\,|\,i}$, but is composed of covariances R_k from lag 2 to 2i. Matrix A is found by introducing Eq. (9), Eq. (10) in Eq. (12) and solving for A:

$$A = {O_i}^+ T_{2\,|\,i+1} {\Gamma_i}^+ = {S_1}^{-1/2} {U_1}^T T_{2\,|\,i+1} V_1 {S_1}^{-1/2}\,, \tag{13}$$

where + denotes the Moore-Penrose pseudo-inverse of a matrix. Matrix C, can be calculated with the following way:

$$[C] = O_i(1{:}\,l,:), \tag{14}$$

Finally, modal parameters can be obtained from matrices A and C. First, the eigenvalues of A, which are the poles of the discrete-time state-space model, have to be related with poles of the continuous-time model λ_k. Then the poles with a positive imaginary component are used to obtain natural frequencies (f_k) and modal damping ratios (ξ_k) [12] and the observed modes, can be computed with Eq. (18), where $[\psi]$, is eigenvector matrix of A.

$$\lambda_k = \frac{ln(\mu_k)}{\Delta t}\,, \tag{15}$$

$$f_k = \frac{|\,\lambda_k\,|}{2\pi}\,, \tag{16}$$

$$\xi_k = -\frac{Re(\lambda_k)}{|\,\lambda_k\,|}, \tag{17}$$

$$[V] = [C][\psi]. \tag{18}$$

2.1 Stabilization of poles

In the SSI-COV method, the system order is indicated by the non-zero singular values of the Toeplitz matrix $T_{1|i}$. In practice, the order can be determined by looking at a gap between two successive singular values [9], however, according to Reynders et al. [19], even the higher singular values that should be zero, in practice present some residual values due to the presence of noise in the system which is also reflected on the output measurements. To overcome this difficulty, it is common to construct a stabilization diagram. The stabilization diagrams are used to discriminate spurious modes, as often these do not achieve stabilization criteria as in the case of the physical poles. Other spurious poles can be identified and eliminated according to physical criteria [20]. For a model order equal to n^*, the resulting poles m^* are compared with all poles in preceding orders $n = n^* - \sigma$, where $\sigma = 1,2,3,\ldots,s$ and s is a positive integer that defines the required stability level [11].

If the comparison of eigenfrequencies, damping ratios and mode shapes are within the present criteria, then the pole is considered stable. For the present study, the criteria to satisfy are:

$$\frac{\left| f_{n*,m*} - f_{n,m} \right| * 100}{f_{n*,m*}} \leq 1\% \tag{19}$$

$$\frac{\left| \xi_{n*,m*} - \xi_{n,m} \right| * 100}{\xi_{n*,m*}} \leq 5\% \tag{20}$$

$$100 * \left(1 - MAC\left(\{V_{n*,m*}\}, \{V_{n,m}\}\right)\right) \leq 2\%. \tag{21}$$

Figure 1 shows that applying the decomposition of singular values of the block Toeplitz matrix $n_{yi}\ by\ n_{yi}$ of output covariances, produces three $n_{yi}\ by\ n_{yi}$ matrices. Afterwards a variable even number of singular values ($2m_1 < 2m_2$) is successively chosen to reconstruct the system matrices O, Γ, A, C and then the modal parameters are estimated through Eqs. (15), (16), (17) and (18). In the figure, two cases are shown: the choice of $2m_2$ singular values, leads to m_2 modes estimates, while the choice of $2m_1$ singular values leads to m_1 modes estimates. Thereafter, those parameters satisfying the stability criteria described by Eqs. (19), (20) and (21) are plotted in the stabilization diagram and the arising vertical alignments of stable poles are representing the physical modes of the model [21].

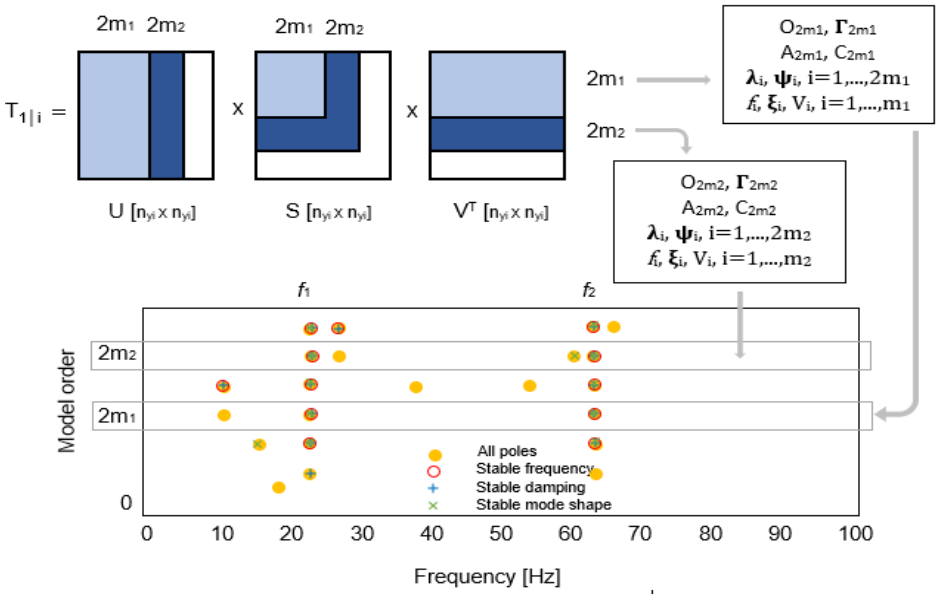

Figure 1. SSI-COV method: Construction of stabilization diagram

2.2 Validation of SSI-COV method

To validate the method, a simulation of experimental data was performed in the programming language Python in order to obtain data similar to those that would be obtained in a dynamic test of measurement of ambient vibrations. This allowed to compare the exact characteristics of the structural model considered in the simulation, which was a beam simply supported at its ends, discretized in 6 elements, each one with length of $1\,m$ (Fig 2). A square section of $0.15\,m$ was set, a modulus of elasticity of the material equal to $1.787 * 10^{10}\ \frac{N}{m^2}$ and concentrated masses in the vertical directions equal to $288.36\,Kg$. In order to reduce the size of the problem the axial degrees of freedom were not considered, and the rotational degrees of freedom were condensed to 5 vertical degrees of freedom [22].

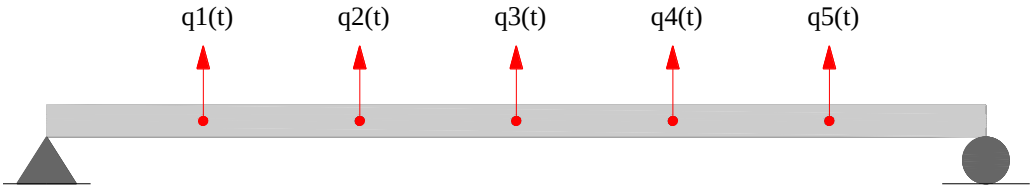

Figure 2. Structural model with five degrees of freedom

From the geometric and material properties, the matrices of masses M and stiffness K of the structure were determined, which turned out to have a size of 5x5 each one. A constant modal damping ratio of 2% is assumed for all modes i. The eigenfrequencies and damping ratios are given in Table 1 and the corresponding eigenmodes are shown in Fig. 3.

Table 1. First five eigenfrequencies *f* and damping ratios **ξ** of the simply supported beam

#	*f* [Hz]	**ξ** [%]
1	2.231	2
2	8.915	2
3	19.933	2
4	34.526	2
5	49.398	2

Time series of vertical accelerations were created in each of the degrees of freedom. These accelerations were obtained from a random excitation. To represent the random vibration, a time series of white noise (mean zero and unit variance) was set with a duration of 5 minutes at a sampling frequency of 400 Hz.

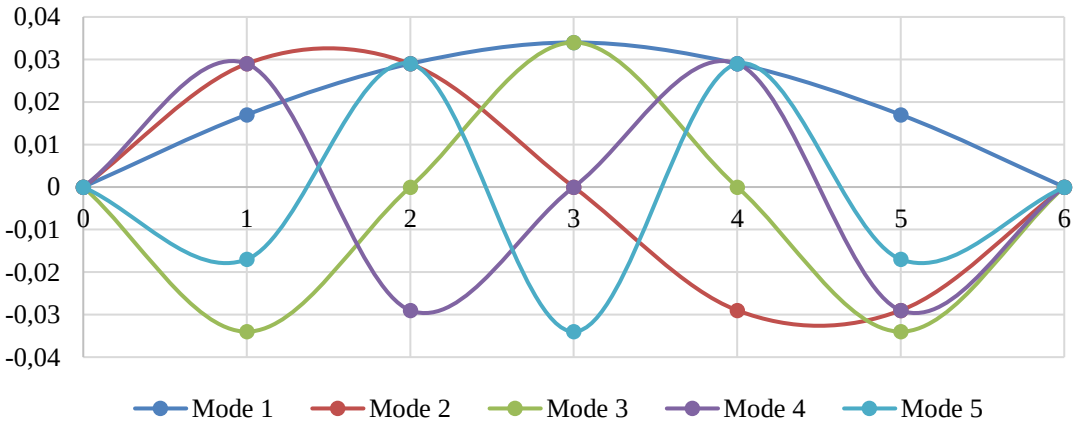

Figure 3. First five mode shapes of the simply supported beam

In order to evaluate the sensitivity of the SSI-COV method, 2 types of simulations were performed, in the first, the noise effect was evaluated, a noise with a mean equal to zero and a variance equal to the intensity of the noise was introduced to the response vector. Three different noise levels were considered: $SNR = 14\ dB$, $SNR = 22\ dB$, and $SNR = 30\ dB$, where SNR is the Signal-to-noise ratio. In the second simulation was evaluated the time duration. In this case, the frequency was maintained at 400 Hz and the random vibration was re-established for 100, 300 and 500 seconds and a $SNR = 10\ dB$ was set. As it was required to identify 5 modes, in the two simulations a maximum order of $n_{max} = 10$ was used. Stabilization was performed for orders equal to $n = 2,4,\ldots,40$ with a stability level of $s = 1$ and the stability criteria detailed in Eq. (19), (20), and (21).

Tables 2, 3 and 4 show the parameters identified in the structure that were obtained through the noise contaminated responses. A high value of SNR indicate that a small amount of signal noise is added to the vibration, while a low SNR indicates that the signal is noise dominant. In practice, acceleration records are frequently contaminated with noise, which can lead to increased error in the estimated modal parameters. The damping is highly sensitive to the quality of the estimated correlation function, which may be distorted by signal noise [14]. This can be seen in the parameters identified: natural frequencies and vibration modes presented low and acceptable errors compared to damping ratios specifically by tracking mode 5, it can be clearly observed how the error increases in magnitude as noise increases.

Table 2. Frequencies identified in the first simulation

Noise	*Mode*	f_{mean} *[Hz]*	f_{std} *[Hz]*	*Error[%]*
(No-noise)	1	2.229	8.375e-05	0.050
	2	8.918	0.000755	0.038
	3	19.929	0.001835	0.019
	4	34.518	0.005303	0.022
	5	49.406	0.00644	0.017
(SNR 30)	1	2.2197	0.000566	0.503
	2	8.9102	0.003763	0.053
	3	19.951	0.001170	0.095
	4	34.619	0.003978	0.270
	5	49.503	0.001267	0.213
(SNR 22)	1	2.2209	0.001267	0.453
	2	8.9004	0.001929	0.164
	3	19.917	0.003896	0.080
	4	34.601	0.002114	0.217
	5	49.678	0.001376	0.567
(SNR 14)	1	2.234	0.00154	0.146
	2	8.905	0.00500	0.104
	3	19.973	0.004838	0.202
	4	35.563	0.264314	3.006
	5	50.343	0.001547	1.914

Table 3. MAC obtained in the first simulation

Mode	*(No-noise)*	*(SNR 30)*	*(SNR 22)*	*(SNR 14)*
1	100%	99.76%	99.45%	99.6%
2	100%	99.98%	98.67%	98.9%
3	100%	99.93%	99.87%	99.9%
4	100%	99.9%	99.37%	97.65%
5	100%	100%	99.9%	96.45%

Table 4. Damping ratios identified in the first simulation

Noise	*Mode*	ξ_{mean} *[%]*	ξ_{std} *[%]*	*Error[%]*
(No-noise)	1	2.010	3.997E-03	0.50
	2	2.032	2.577E-03	1.60
	3	2.054	9.410E-03	2.70
	4	2.020	4.305E-03	1.00
	5	2.005	9.314E-03	0.232
(SNR 30)	1	1.856	0.0166	7.219
	2	1.956	0.0239	2.207
	3	2.147	0.0086	7.327
	4	2.136	0.0289	6.780
	5	2.549	0.0134	27.429
(SNR 22)	1	2.132	0.0281	6.625
	2	2.129	0.0321	6.451
	3	1.856	0.0150	7.154
	4	2.116	0.0218	5.808
	5	3.366	0.0389	68.339
(SNR 14)	1	1.855	0.0898	7.206
	2	1.917	0.0111	4.145
	3	2.118	0.0329	5.902
	4	3.753	0.0567	87.650
	1	1.855	0.0898	7.206

In the SSI-COV method, the time duration is assumed infinite long, however, infinite data is not possible in reality. The second simulation was carried out in order to violate that assumption. Tables 5, 6 and 7 show the parameters identified by performing three variations in measurement duration. Results again show that the method is robust in identifying natural frequencies and vibration modes. In the case of damping ratios, it is shown that time duration affects the estimate of this parameter. A shortening of the duration of the vibration records yield an increase in the bias and variance error for the correlation function estimates [14].

Table 5. Frequencies identified in the second simulation

Time duration	*Mode*	f_{mean} *[Hz]*	f_{std} *[Hz]*	*Error[%]*
100 [Sec]	1	2.235	0.000769	0.203
	2	8.903	0.010457	0.133
	3	19.948	0.121414	0.078
	4	35.280	0.571537	2.184
	5	51.678	0.79612	4.617
300 [Sec]	1	2.226	0.00141	0.1916
	2	8.916	0.00253	0.0127
	3	19.984	0.02258	0.2557
	4	34.509	0.15816	0.0494
	5	49.833	0.25417	0.8806
600 [Sec]	1	2.2382	0.000259	0.3227
	2	8.9220	0.009725	0.0785
	3	19.954	0.010024	0.1053
	4	34.386	0.029387	0.4054
	5	49.456	0.18937	0.1174

In table 7, it is observed that for mode 5 the method failed to identify the damping rate when time duration was 100 [sec] and 300 [sec] also errors decreased as duration increased. Finally, the two simulations carried out allowed to determine that the damping ratios are the most sensitive parameter due to the changes in the correlation function and the similarity between the identified parameters and the theoretical values made it possible to validate the method.

Table 6. MAC obtained in the second simulation

Mode	*100 [Sec]*	*300 [Sec]*	*600 [Sec]*
1	97.36%	99.90%	99.95%
2	98.95%	99.36%	99.95%
3	98.76%	98.90&	98.97%
4	99.13%	99.20%	99.56%
5	99.24%	99.50%	100%

Table 7. Damping ratios identified in the second simulation

Time duration	*Mode*	ξ_{mean} *[%]*	ξ_{std} *[%]*	*Error[%]*
100 [Sec]	1	2.4934	0.0282	24.667
	2	1.9682	0.0174	1.5920
	3	2.3380	0.2135	16.902
	4	3.7800	0.2621	89.000
	5	-	-	-
300 [Sec]	1	2.2513	0.0108	12.563
	2	2.0218	0.0364	1.088
	3	1.9681	0.0927	1.5971
	4	2.5124	0.0886	25.619
	5	-	-	-
600 [Sec]	1	1.9338	0.0203	3.3120
	2	1.9881	0.0157	0.5952
	3	2.0230	0.0171	1.1479
	4	2.0040	0.0141	0.2003
	5	2.7361	0.0457	36.805

3 Brief description of the case study

The SSI-COV method was implemented to identify frequencies and damping ratios of the D38 concrete block of the Itaipú Hydroelectric Dam. This block is located in section D of the dam as shown presented in Fig. 4, and it's equipped with a 3-channel sensor. This sensor is configured to acquire acceleration signals with a sampling frequency of 200 Hz and produce 24-hour time series. To apply the method, data of 19/05/2019 were collected from 10:00 a.m. to 10:30 a.m. with a total of 360000 samples in each direction (Longitudinal, transversal and vertical). Fig. 5 shows the time history of collected acceleration. As the block is only equipped with only one sensor, the information was not enough to identify vibration modes.

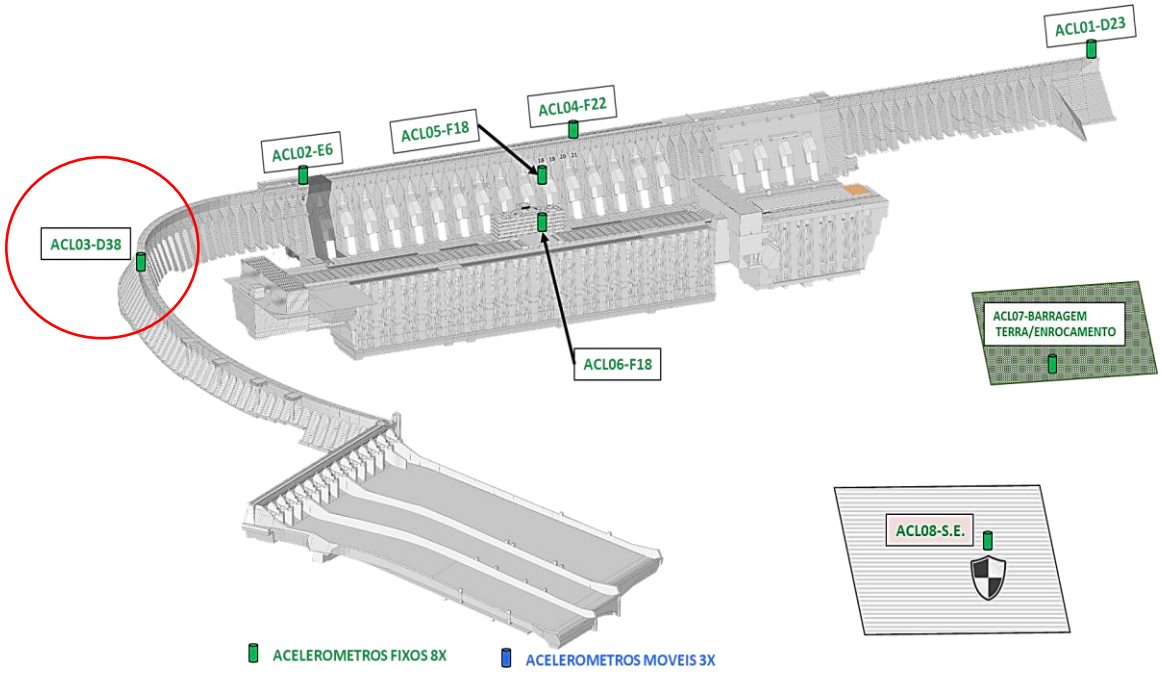

Figure 4. Itaipú accelerograph network (CEASB, 2019)

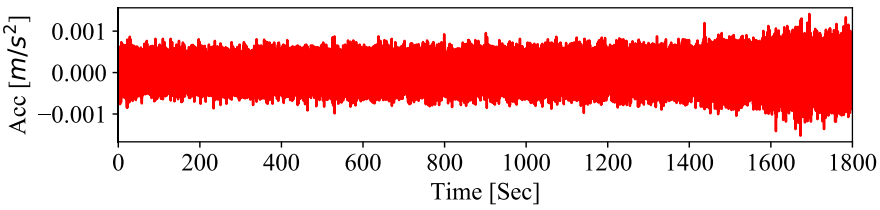

(a) Longitudinal direction

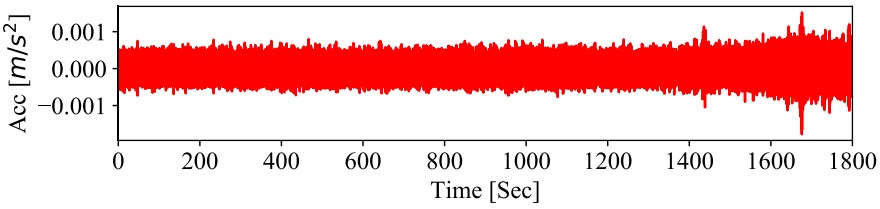

(b) Transversal direction

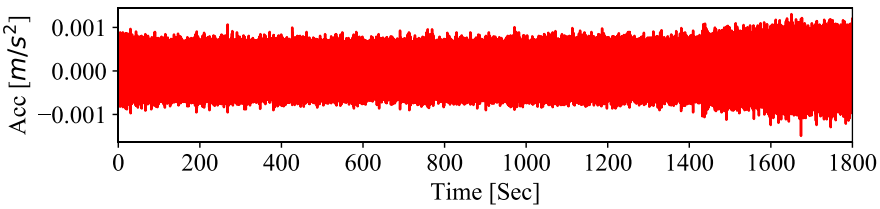

(c) Vertical direction

Figure 5. Acceleration time series

3.1 Data preprocessing

The acceleration data measured in block D38 were pre-processed for assessing the frequency content of the response in the recordings. First, the obtain dataset were decimated in order to obtain a final sampling frequency of 40 Hz. Then, the power spectral densities (PSD) of each signal was determined using the Welch's method. The power spectral density of the signal is suitable to represent transient signals that are similar to pulsation and with total finite energy [12]. PSD of the signal can be determined by:

$$G_{xx}(f) = \frac{2}{T} E\left[\,\left|\, X(f,T) \,\right|^2\right], \tag{22}$$

where E is a mathematical expectancy, f is the frequency, $X(f,T)$ is the finite Fourier transform of the signal $x(t)$ in a window of duration T, determined by:

$$X(f,T) = \int_0^T x(t) e^{-i2\pi f t} dt\,, \tag{23}$$

where $i = \sqrt{-1}$ the imaginary number and t the time.

Figure 6. shows the PSDs of the vibration signals measured by the ACL03-D38 accelerometer. Python 3.7's signal.welch function was used in the analysis, with the following input variables: acceleration times series with a duration of 30 minutes, the sampling frequency (Fs = 40 Hz), Window (hanning), length of each segment (nperseg = 2048), Number of points to overlap between segments (noverlap = 1024), length of the FFT (nfft = 2048).

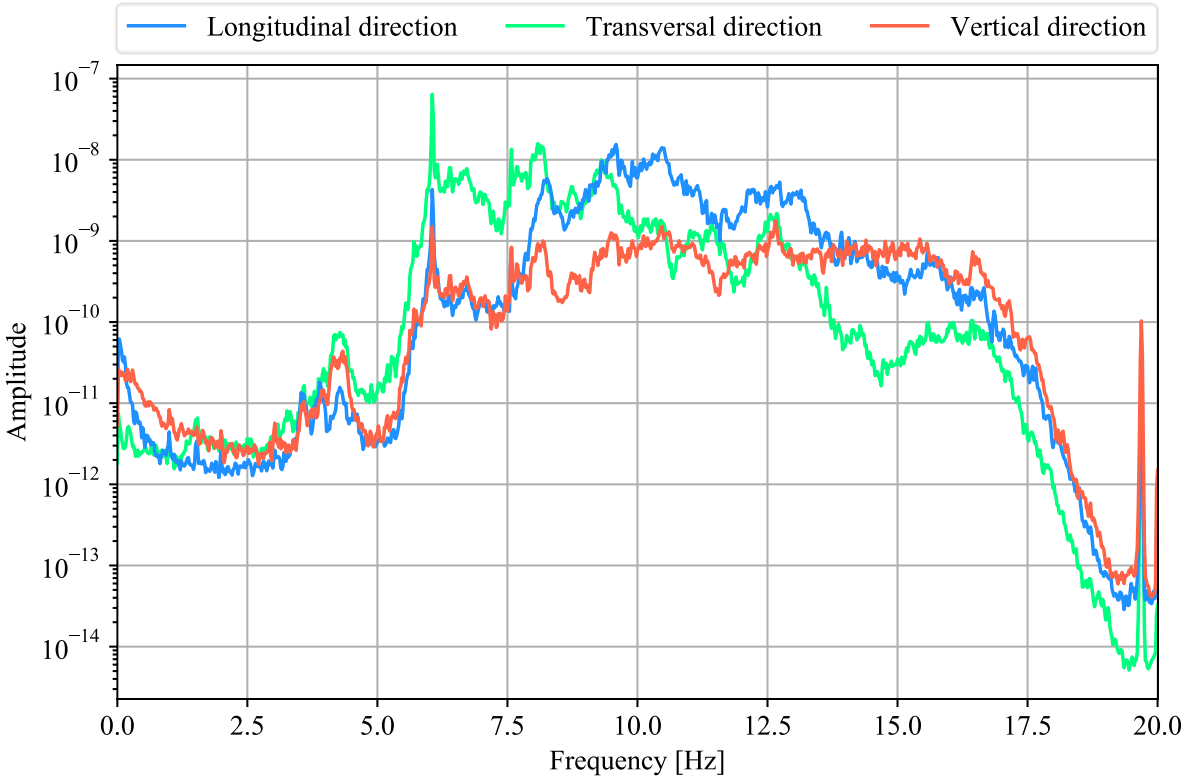

Figure 6. PSDs of ACL03-D38

The Averaged Normalized Power Spectral Density (ANPSD) [24], is useful for avoiding the analysis of several graphs in each degree of freedom instrumented. The ANPSD can be determined as:

$$ANPSD(w) = \frac{1}{l}\sum_{i=1}^{l} NPSD_i(w), \tag{24}$$

Where l is the number of degrees of freedom instrumented and $NPSD_i$ are the normalized spectra, which are obtained by dividing the estimate of the PSD_i by the sum of their N ordinates.

$$NPSD_i(w) = \frac{PSD_i(w)}{\sum_{k=1}^{N} PSD(w_k)}. \tag{25}$$

With the calculated spectral density functions, the ANPSD standardized mean spectrum is determined. The spectrum presented in Fig. 7 corresponds to the mean of the PSDs shown in Fig. 6, normalized according to equation (24).

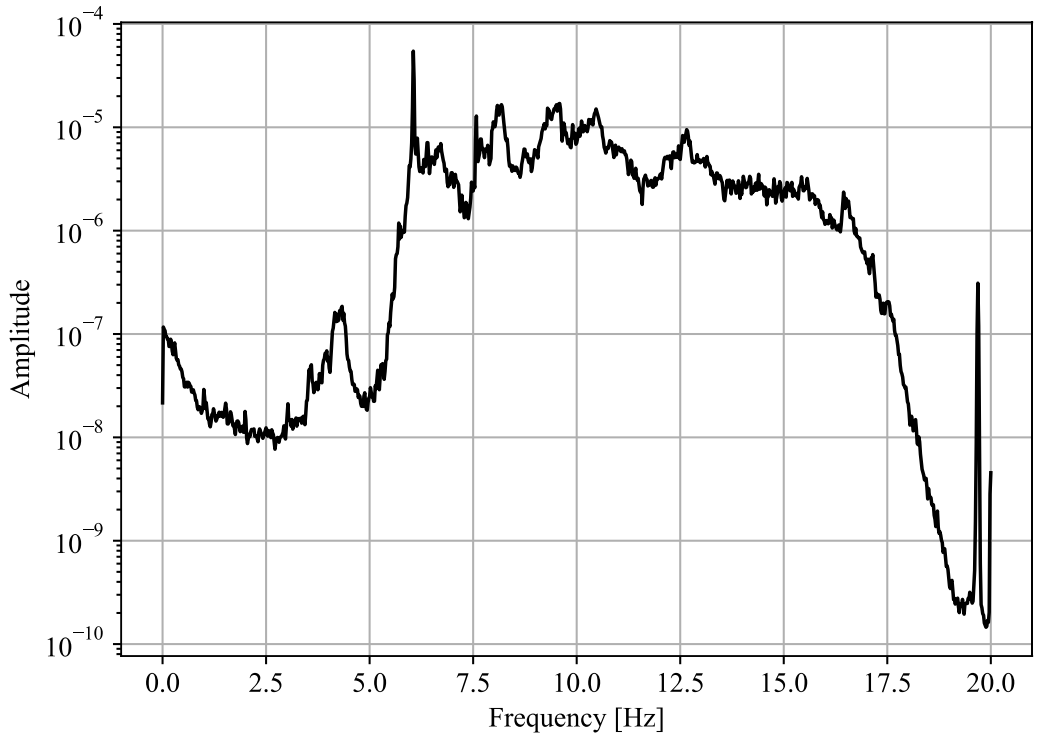

Figure 7. ANPSD of ACL03-D38

4 Results and discussion

The most important aspect observed in this application was the identification of the maximum order of the model order. In order to identify the frequencies and damping rat in the concrete block, different executions of the algorithm were carried with different orders. This methodology was performed because it was not possible to identify in the singular values diagram in Fig. 8. a gap between two successive singular values. In all executions, a stability level of s=2 and n = 2,4, ...,150 was used. The set of values adopted for the maximum order were: $n_{max} = [10,20,30, \ldots,60]$ and to compute the state transition matrix A was used Eq. (11).

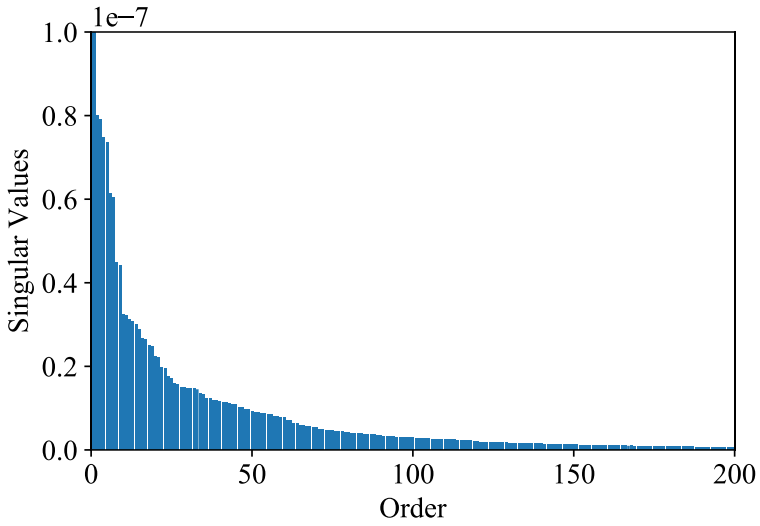

Figure 8. Singular values diagram

Figure 9. and 10, shows the stabilization diagrams obtained for each case. ANPSD it is plotted over the stabilization diagram as a visual aid to select the stable frequencies. The stabilization criteria used were those detailed in the Eq. (19) and Eq. (20). Using different orders, it could be observed that values higher than $n_{max} = 40$, leads to the appearance of spurious modes associated to the noise content of measurements. For the case study, it was determined that a value of $n_{max} = 30$ was suitable, thus, the SSI-COV method provided information of the first 14 vibration modes. Figure 11., shows a zoom of the stabilization diagram using $n_{max} = 30$, for orders between 80 and 150, in which stabilization was achieved. Also, can be observed in Fig. 11 that SSI-COV method is able to correctly identify closely spaced modes, for example, those close to 8 [Hz].

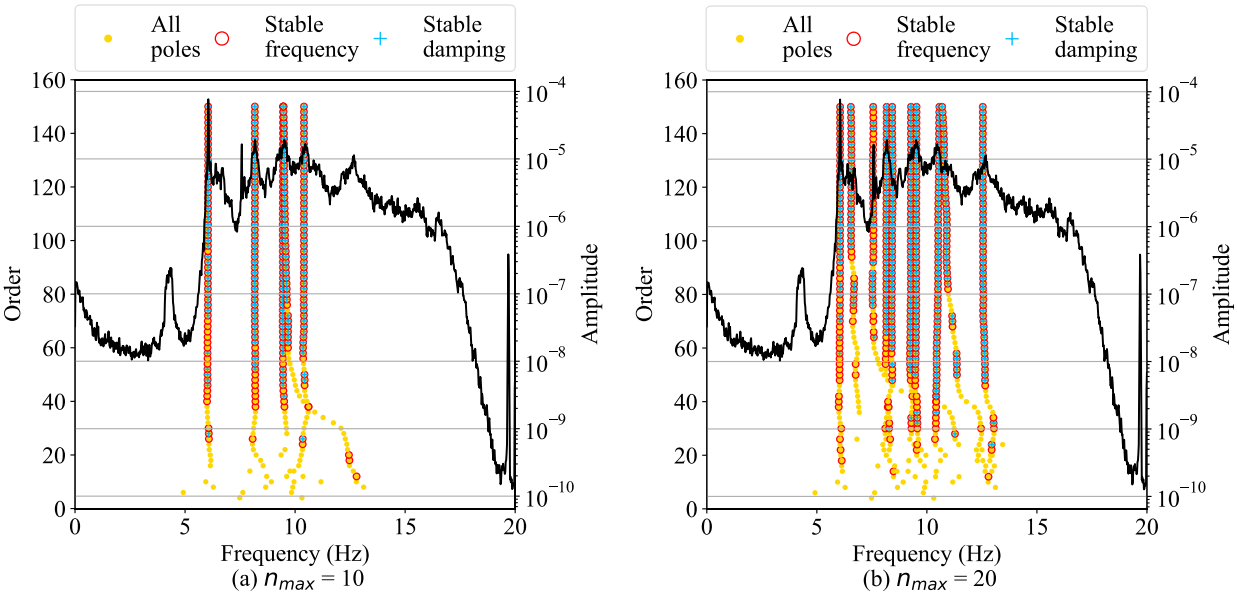

Figure 9. Stabilization diagram for different n_{max} values: 10, 20

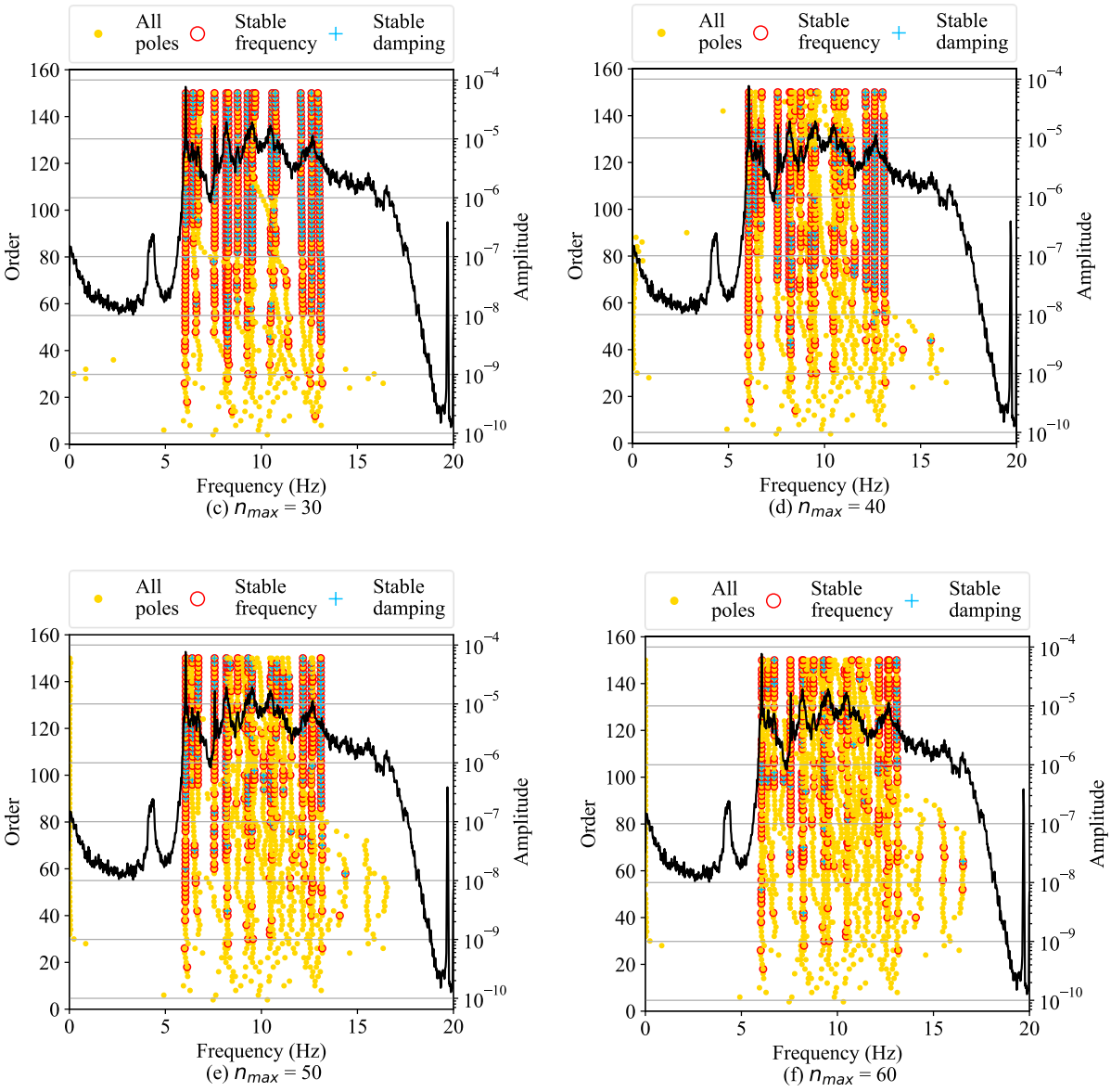

Figure 10. Stabilization diagram for different n_{max} values: 30, 40, 50, 60

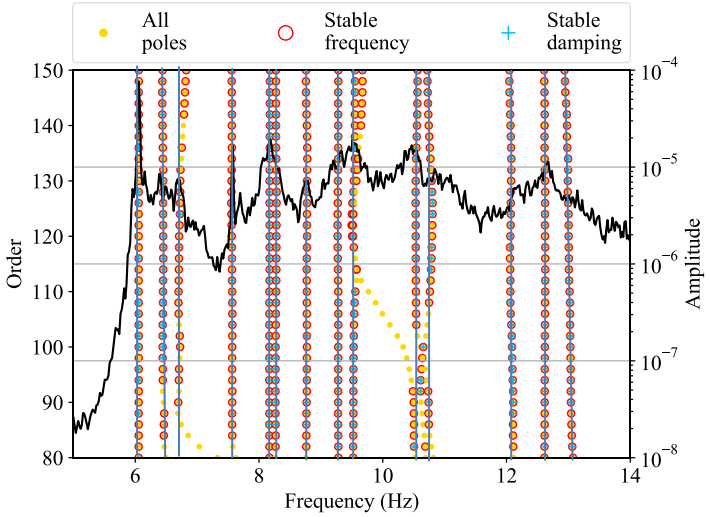

Figure 11. Stabilization diagram for $n_{max} = 30$

After the value of n_{max} was set, the identification process was performed computed the state transition matrix A as described in Eq. (13). Tables 8 and 9 show the identified parameters using statistical parameters such as minimum and maximum values, mean and their corresponding standard deviation. *Frequency 1.* and *Damping 1.* refers to the frequencies and damping ratios obtained by computed matrix A with Eq. (11), while *Frequency 2.* and *Damping 2.* refers to the parameters obtained by computed matrix A with Eq. (13). The natural frequencies identified in the two cases are very similar; however, those obtained using Eq. (11) show less variability than those obtained with Eq. (13). For each mode, the relative standard deviation of case 1 is lower than case 2. The maximum relative standard deviation for the two cases was presented in the mode 3, for case 1. was 0.25%, while for case 2. was 0.59%.

Table 8. Frequencies identified in the concrete block D38.

Mode	*Case 1. Frequency 1. [Hz]*			*Case 2. Frequency 2. [Hz]*		
	$f_{[Min;Max]}$	f_{mean}	f_{std}	$f_{[Min;Max]}$	f_{mean}	f_{std}
1	[6.0357; 6.0570]	6.0520	0.00036	[6.0354; 6.0570]	6.0525	0.00627
2	[6.4356; 6.4531]	6.4465	0.00395	[6.4349; 6.4534]	6.4458	0.00527
3	[6.6991; 6.8224]	6.7361	0.01748	[6.6983; 6.8227]	6.7362	0.03958
4	[7.5166; 7.5696]	7.5604	0.00169	[7.5212; 7.5694]	7.5609	0.00917
5	[8.1546; 8.1756]	8.1695	0.00032	[8.1544; 8.1757]	8.1695	0.00428
6	[8.2436; 8.2843]	8.2677	0.00174	[8.2413; 8.2847]	8.2687	0.01156
7	[8.7583; 8.7801]	8.7713	0.00271	[8.7581; 8.7803]	8.7716	0.00555
8	[9.2609; 9.3033]	9.2774	0.00060	[9.2672; 9.2834]	9.2779	0.00393
9	[9.4984; 9.6732]	9.5514	0.00445	[9.4964; 9.6729]	9.5492	0.04640
10	[10.4843; 10.633]	10.5447	0.00193	[10.4820; 10.6317]	10.5413	0.03754
11	[10.6496; 10.803]	10.7591	0.00431	[10.6379; 10.8047]	10.7522	0.04143
12	[12.0450; 12.160]	12.0838	0.00090	[12.0455; 12.1629]	12.0833	0.02825
13	[12.6062; 12.628]	12.6189	0.00085	[12.6066; 12.6281]	12.6190	0.00534
14	[12.9370; 13.103]	13.0311	0.00190	[12.9371; 13.1039]	13.0309	0.04655

Table 9. Damping ratios identified in the concrete block D38.

Mode	*Case 1. Damping 1. [%]*			*Case 2. Damping 2. [%]*		
	$\xi_{[Min;Max]}$	ξ_{mean}	ξ_{std}	$\xi_{[Min;Max]}$	ξ_{mean}	ξ_{std}
1	[0.2400; 0.3549]	0.32390	0.036	[0.2388; 0.3548]	0.31165	0.043
2	[3.9505; 4.9539]	4.29042	0.395	[3.9471; 4.9549]	4.29021	0.388
3	[0.3453; 4.8641]	1.37237	0.748	[0.5288; 4.8211]	2.27996	2.049
4	[0.2584; 1.0724]	0.57311	0.169	[0.2616; 0.8359]	0.53227	0.175
5	[1.4014; 1.6175]	1.42328	0.032	[1.4001; 1.6365]	1.42292	0.033
6	[1.5696; 2.2074]	1.89665	0.174	[1.5987; 2.2138]	1.89182	0.180
7	[0.8550; 1.9053]	1.17713	0.188	[0.8888; 1.4661]	1.16465	0.271
8	[1.5846; 1.8304]	1.64582	0.058	[1.5804; 1.7888]	1.64573	0.061
9	[0.1251; 1.9883]	1.36273	0.438	[0.2378; 2.0129]	1.36078	0.445
10	[1.1485; 2.0989]	1.74104	0.191	[1.0303; 1.9465]	1.73458	0.193
11	[2.0181; 3.9450]	2.84762	0.430	[2.0955; 3.9464]	2.95531	0.512
12	[0.7117; 1.3054]	1.21452	0.090	[0.7124; 1.3070]	1.20039	0.119
13	[1.0354; 1.3903]	1.12222	0.084	[1.0352; 1.4198]	1.12514	0.085
14	[1.7383; 2.5023]	2.05335	0.190	[1.7447; 2.5036]	2.06549	0.200

For damping ratios, the values obtained are similar in both cases in most modes, however the same behavior occurs, the variability of the values for case 1. are lower than those for case 2. in most modes. The maximum relative standard deviation for damping ratios for both cases was presented in the mode

3, for the case 1. was 54.5% while for case 2. was 89.87%. These results allow us to define an advantage in data accuracy when carrying out the identification process applying the shift property of the observability matrix Eq. (11). In terms of computational cost, both cases achieved stability after an order of 80, however, the computational time for case 2. was greater because the Toeplitz matrices $[T]_{1\,|\,i}$ and $[T]_{2\,|\,i+1}$ must be calculated, while for case 1. Only the Toeplitz matrix $[T]_{1\,|\,i}$ is necessary.

5 Final considerations

The SSI-COV method was applied in the identification of modal parameters of a concrete block of the Itaipu Hydroelectric Dam. The simulations performed to validate the method showed that the most sensitive parameter to distortions and changes in the correlation function are the damping rates. These distortions and changes in the correlation function were reflected by adding noise to the response and altering the measurement time.

In the identification of natural frequencies and damping ratios of the concrete block, the method provided information of the first 14 vibration modes and showed its ability to identify quite close modes.

The two alternatives offered by the method to compute the state transition matrix [A], were used in the identification process and it could be determined that applying the shift property of the observability matrix is more advantageous in terms of precision and computational cost.

Acknowledgements

The authors acknowledge UNILA (University of Latin American Integration) for financial support, ITAIPÚ for acceleration data and CEASB for laboratories to perform simulations.

References

[1] S. Pereira, F. Magalhães, J. Gomes, A. Cunha, J. Lemos, Dynamic monitoring of a concrete arch dam during the first filling of the reservoir. Engineering Structures, Vol 174, pp. 548-560, 2018.
[2] L. Vargas. Propuesta de plan de monitoreo del comportamiento dinámico para la salud structural del nuevo puente Gómez Ortiz en la vía Girón Zapatoca. Msc Tesis. Universidad Industrial de Santander. 2016.
[3] M. Rodriguez. Análisis modal operacional: Teoría y practica. Sevilla, España, 2005.
[4] B. Cauberghe. Applied frequency domain system identification in the field of traditional and operational modal analysis. 2004.
[5] A. Cunha, E. Caetano. Experimental Modal Analysis of Civil Engineering Structures. Sound and Vibration. pp. 12-20, 2006.
[6] C. Rainieri, G. Fabbrocino. Operational modal analysis of civil engineering structures. New York: Springer. p. 143, 2014.
[7] R. Brincker, L. Zhang, P. Andersen. Modal identification from ambient responses using frequency domain decomposition. In: IMAC 18, International modal analysis conference. San Antonio, USA, 2000.
[8] B. Peeters, H. Van der Auweraer. Polymax: a revolution in operational modal analysis. In: IOMAC, international operational modal analysis conference. Copenhagen, Denmark, 2005.
[9] B. Peeters. System identification and damage detection in civil engineering. Katholieke Universiteit Leuven, 2000.
[10] J. García, J. Soria, Ivan. Diaz, F. Tirado. Ambient modal testing of a double-arch dam: the experimental campaign and model updating. Journal of Physics: Conference Series 744, 2016.
[11] K. Kvale, O. Oiseth, A. Ronnquist. Operational modal analysis of an end-supported pontoon bridge. Engineering Structures. pp. 410-423, 2017.

[12] F. Magalhães, A. Cunha. Explaining operational modal analysis with data from na arch bridge. Mechanical Systems and Signal Precessing. pp. 1431-1450, 2011.
[13] M. Xu, L. Santos, T. Vieira. Modal identification of bridges based on Continuous Dynamic Monitoring. 8th European Worshop On Structural Health Monitoring. Bilbao, Spain, 2016.
[14] A. Bajric, J. Hogsberg, F. Rudinger. Evaluation of damping estimates by automated Operational Modal Analysis for offshore wind turbine tower vibrations. pp. 153-163, 2018.
[15] C. Rainieri, G. Fabbrocino, G.M. Verderame. Non-destructive characterization and dynamic identification of a modern heritage building for serviceability seismic analyses. NDT&E International. pp. 17-31, 2013.
[16] PV. Overschee, BD. Moor. Subspace identification for linear systems- theory, implementation, applications. Kluwer Academic Publishers, 1996.
[17] S. Y. Kung. A new identification and model reduction algorithm via singular value decomposition. In proceedings of the 12th Asilomar Conference on Circuits, Systems and Computers. pp. 705-714, Asilomar, CA, USA, 1978.
[18] H. P. Zeiger, A.J. McEwen. Approximate linear realization of given dimension via Ho's algorithm. IEEE Transactions on Automatic Control, AC-19(2), 153, 1974.
[19] E. Reynders, R. Pintelon, G. De Roeck. Uncertainty bounds on modal parameters obtained from stochastic subspace identification. Mechanical Systems and Signal Processing. Vol. 22, pp. 948-969, 2008.
[20] C. Rainieri, G. Fabbrocino. Influence of model order and number of block rows on accuracy and precision of modal parameter estimates in stochastic subspace identification. Int. J. Lifecycle Performance Engineering. Vol. 1, 2014.
[21] K. Tatsis. Structural Health Assessment through Vibration Monitoring on FPSOs. Msc Tesis. Delf University of Technology. Netherlands, 2016.
[22] I. Gomez. Caracterización dinámica experimental de puentes de hormigón simplemente apoyados a partir de mediciones de vibración Ambiental. Msc Tesis. Universidad Industrial de Santander, 2010.